RESEARCH ARTICLE | NOVEMBER 15 2022

Thermal effects on TiN/Ti/HfO_2/Pt memristors charge conduction

F. Jiménez-Molinos ✉ ; G. Vinuesa ; H. García ; A. Tarre ; A. Tamm ; K. Kalam ; K. Kukli ; S. Dueñas ; H. Castán ; M. B. González ; F. Campabadal ; J. B. Roldán

J. Appl. Phys. 132, 194501 (2022)
https://doi.org/10.1063/5.0104890

Journal of Applied Physics ARTICLE scitation.org/journal/jap

Thermal effects on TiN/Ti/HfO_2/Pt memristors charge conduction

Cite as: J. Appl. Phys. **132**, 194501 (2022); doi: 10.1063/5.0104890
Submitted: 4 August 2022 · Accepted: 22 October 2022 ·
Published Online: 15 November 2022

F. Jiménez-Molinos,[1,a)] G. Vinuesa,[2] H. García,[2] A. Tarre,[3] A. Tamm,[3] K. Kalam,[3] K. Kukli,[3] S. Dueñas,[2] H. Castán,[2] M. B. González,[4] F. Campabadal,[4] and J. B. Roldán[1]

AFFILIATIONS

[1]Departamento de Electrónica y Tecnología de Computadores, Universidad de Granada, Facultad de Ciencias, Avd. Fuentenueva s/n, 18071 Granada, Spain
[2]Departamento de Electrónica, Universidad de Valladolid, Paseo de Belén 15, 47011 Valladolid, Spain
[3]Institute of Physics, University of Tartu, W. Ostwaldi 1, 50411 Tartu, Estonia
[4]Institut de Microelectrònica de Barcelona, IMB-CNM (CSIC), Carrer dels Til·lers s/n, Campus UAB, 08193 Bellaterra, Spain

a)Author to whom correspondence should be addressed: jmolinos@ugr.es

ABSTRACT

TiN/Ti/HfO_2/Pt resistive switching devices have been fabricated, measured, and modeled. After programming the devices in the low resistance state, the current–voltage characteristic below the reset switching voltage was measured at different temperatures (from 90 to 350 K). A weak but complex temperature dependence was obtained for several voltage regimes. These memristors belong to a wider set known as valence change memories, whose conductance is determined by the formation of conductive filaments (CFs) linked to a high density of oxygen vacancies in a dielectric sandwiched between two metal electrodes. This usually leads to ohmic conduction in the low resistance state. However, a non-linear current dependence has been also observed in the measured devices, in addition to symmetric current–voltage curves for positive and negative biases in the 0–0.6 V voltage range. Three different thermal dependences have been considered for explaining the whole set of experimental data. Two of them are linked to ohmic filamentary conduction; the CF shows a conductivity enhancement due to thermally activated mechanisms at low temperatures; on the contrary, a CF conductivity degradation is observed at the higher temperatures. Finally, an additional slightly higher value for the non-linear current component as the temperature rises has also been taken into account. A semiempirical compact model has been implemented including these conduction mechanisms and their corresponding temperature dependences, the device has been simulated in LT-Spice and the experimental currents have been correctly reproduced.

I. INTRODUCTION

Memristors have emerged as key elements in non-volatile memories, neuromorphic chips for the hardware implementation of artificial intelligence systems,[1,2] and cryptographic circuits.[3] Redox-based memristive devices or Resistive Random Access Memories (RRAMs) are two terminal devices whose resistance can be changed by applying appropriate voltage/current signals.[4–6] Without external voltage, the programmed resistance remains and, therefore, the devices can be used as non-volatile memory elements. After a usually required initial forming process, the devices can be switched between two distinguishable conduction states: the low resistance state (LRS) and the high resistance state (HRS), although intermediate states are also allowed in a controllable form in some kind of switching devices.[4,5,7] The transition from LRS to HRS is called reset, while the opposite process is known as set. There is a wide variety of insulators in metal–insulator–metal (MIM) where resistive switching (RS) is observable. There are two main types of RRAMs. Those based on the valence change memories (VCMs) whose RS mechanism is linked to oxygen ions/vacancies motion and in which the conductive filament (CF) is formed by oxygen vacancies,[8,9] and the so-called conductive bridge RRAMs, whose CF formation involves metal cations redox reactions.[8] In this work, we will focus on TiN/Ti/HfO_2/Pt devices, which belong to the first kind, also known as OxRAMs.

Among the wide variety of metal oxides that exhibit RS, HfO_2 devices are outstanding candidates due to their good performance

and CMOS technology compatibility. Therefore, many studies on HfO_2 memristors with different electrode materials have been published. Usually, in the quasistatic operation regime, the devices are characterized by means of I–V plots, obtained by measuring the current through the devices when applying a voltage ramp to them. To characterize the electron conduction, a unique electron transport mechanism is usually chosen according to the measured I–V characteristics, although the temperature dependence analysis is also needed to determine the predominant charge conduction mechanism,[10,11] i.e., measurement of I–V curves at different temperatures is required.

Moreover, a complete device model also needs to include the temperature dependence, considering that RS physical mechanisms are thermally activated. In this work, we have addressed both tasks: the device current temperature dependence in the LRS has been characterized and modeled.

In HfO_2 based VCMs, conduction is assumed to take place through energy states introduced by oxygen vacancies. There is a vacancy rich region, in which traps are very close or even form a subband (conductive filament) with an ohmic behavior for electron conduction.[12,13] The distance between the nearest trap to the cathode would control the trap-assisted tunnel current.[10] In the HRS, this distance (gap) is higher than in the LRS. Furthermore, constrictions in the filament could also introduce a tunnel barrier in the conduction path,[14] whose effect on the current is modeled with the quantum point contact (QPC) model.[15] As far as the tunnel transmission through the gap or constriction approaches one, the conduction tends to be ohmic.[14,15] By means of *ab initio* simulations, a microscopic picture about electron transport in oxide-based memristive devices has been recently depicted in-depth.[11] According to this study, the subband energetic position is close to the Fermi level. As a consequence, the defect states introduced by the positively charged vacancies can be occupied by electrons, the charge density is reduced, and the subband is pinned to the Fermi level.[11] On the other hand, near the electrode with the highest work function, a depletion zone is formed because the oxygen vacancies closest to the electrode introduce unoccupied trap states above the Fermi level. Therefore, two regions can be distinguished along the insulator: the conductive filament and the depletion zone. In the case of deep defect states (such as those in $Ti/HfO_2/Pt$ devices), electrons have to tunnel through this depletion zone between the electrode and the conductive filament tip. In the LRS, the higher concentration of these unoccupied charged oxygen vacancies contributes to lower the depletion zone length[11] (i.e., the tunneling distance).

In fact, several conduction mechanisms could take place simultaneously and, therefore, a generalized and analytically versatile current expression was proposed for compact modeling purposes[16] (Stanford Model, SM). The SM provides a non-linear I–V dependence (by means of a hyperbolic sine function) even in the LRS, with null gap. A series resistance is sometimes added to the SM in order to account for the CF conduction and to fit I–V curves better.[17,18]

There are several previous studies on the temperature effects on HfO_2 RS devices. Prócel *et al.*[14] measured the current in the LRS and HRS from 298 to 468 K in $TiN/HfO_2/Hf/TiN$ devices, and they found a very weak temperature dependence in the LRS at 0.1 V. A stronger temperature dependence of the LRS resistance was found in $TiN/HfO_2/TiN$ devices[19] over a similar temperature range. A much higher current variation was measured in $Pt/Al_2O_3/HfO_x/Er/Pt$ in the temperature range 40–350 K,[20] which was related to an enhancement of trap-assisted tunneling involving phonons.[20] Temperature dependent switching behavior has also been characterized at extremely low temperatures (4 K),[21] performing RS cycles at different temperatures resulting in CFs and traps with several barrier heights.[21] According to Ref. 22, cycling induces a higher temperature dependence in the measured resistances in relation to the variation observed without performing RS cycles, although this effect is higher in the HRS. In that work, $TiN/HfO_2/Ti/TiN$ devices were employed, and a metallic-like behavior was observed in the LRS (resistance increased as the temperature rose) in the temperature range (213–413 K).[22] In the present study, we have measured the LRS current–voltage characteristics in the temperature range 90–350 K without cycling so that the CF shape can be assumed to remain unchanged and the temperature effects can be attributed to the charge conduction mechanisms and not to the switching processes. A weak and complex thermal dependence has been obtained, with different trends at low and high voltage operation regimes.

The paper is organized as follows: in Sec. II, we introduce the device fabrication and measurement details. The experimental data obtained are shown in Sec. III, while the modeling developments are tackled in Sec. IV; finally, we wrap up with the main conclusions in Sec. V.

II. DEVICE DESCRIPTION AND MEASUREMENT SETUP

Cross-point $TiN/Ti/HfO_2/Pt$ devices were fabricated on Si wafers with a thermally grown 200 nm SiO_2 layer. First, the bottom electrode, consisting of a 100 nm-thick Pt layer on a 5 nm Cr adhesion layer, was deposited and patterned by photolithography and lift-off. Then, a 13 nm thick HfO_2 film was deposited by Atomic Layer Deposition (ALD) in a Picosun TM R-200 Advanced ALD System, using $Hf[N(C_2H_5)(CH_3)]_4$ (TEMAH) and O_2 plasma as the hafnium and oxygen precursors, respectively, and N_2 as the carrier and purge gas. ALD cycle times were 0.3–8.0–15.0–8.0 s for the sequence TEMAH pulse–N_2 purge–O_2 plasma pulse–N_2 purge, respectively. The films were x-ray amorphous, as confirmed by diffraction measurements. The defective nature of the solid medium here is to be considered, not only due to the disordered lattice structure, but also because of the presence of chemical residues. It is known from preceding studies on HfO_2 films grown in a similar plasma-assisted process[23] that the content of carbon and nitrogen can exceed 3–6 at. %. In addition, due to the presence of hydrogen in TEMAH, the residual hydrogen in the HfO_2 grown using TEMAH may reach 2–3 at. %.[24] Besides residuals, oxygen vacancies, inevitably present in such oxides, cause electronic trap states in the bandgap of HfO_2.[25]

After the HfO_2 deposition, the top electrode, which consisted of 200 nm thick TiN on 10 nm Ti layer, was deposited by magnetron sputtering and patterned by photolithography and lift-off. Finally, the electrical contact area to the bottom Pt electrode was defined by photolithography and dry etching of the HfO_2 layer. The resulting cross-point structures have an area of $60 \times 60\,\mu m^2$.

In earlier studies on such structures, reproducible bipolar RS current–voltage behavior has been established.[26]

The electrical measurements were carried out by means of a Hewlett-Packard Semiconductor Analyzer 4155B. Voltage bias was applied to the top electrode while the bottom electrode remained grounded. The measurements were performed in a wide temperature range, from 77 to 350 K in an Oxford Instruments Cryostat DM1710 and monitored by an Oxford Instruments Temperature Controller ITC 503. The equipment was connected to a computer via GPIB interface and controlled using Agilent VEE software. More than 20 devices were tested at room temperature, and all of them showed the same conduction mechanisms and *I*–*V* curves over the voltage ranges. Figure 1 shows experimental RS cycles measured at room temperature before and after performing the study detailed in Sec. III. As can be seen, the studied devices show clockwise resistive switching,[26] that is, set is obtained by the application of a negative voltage, while a positive voltage ramp is applied for the reset process. Finally, it is remarkable that the current in the LRS does not change significantly after the experiment and only the set voltage shows a noticeable cycle-to-cycle variability.

III. EXPERIMENTAL RESULTS

After a set process at 77 K, the *I*–*V* characteristics were measured at different temperatures (from 90 to 350 K) with a maximum applied voltage of 0.7 V, which is lower than the average reset voltage (higher than 1 V). Therefore, we can assume that the microscopic filament configuration remains almost constant throughout the experiment. Figure 2 shows the experimental *I*–*V* curves. As can be noted, different temperature dependences have been obtained. For voltages below 0.3 V, the current shows a slight increase as temperature rises. However, at the highest measured voltages (from 0.4 to 0.7 V, approximately), a different behavior is observed: the current also slightly increases with the temperature but shows a maximum around 190–200 K; for higher temperatures, the current decreases if the temperature rises. This is not a simple dependence that can be captured by a single conduction mechanism, so several mechanisms (with different temperature dependences) should be considered for modeling. This fact is highlighted in Fig. 3, where the current from Fig. 2 has been plotted vs the temperature for low (a) and high (b) voltages.

In the Arrhenius plot shown in Fig. 3(a) for a low applied voltage (0.05 V), the data do not show a single linear trend corresponding to a unique thermally activated conduction mechanism, but two different growing trends are observed. On the other hand, Fig. 3(b) illustrates the above commented current dependence on the temperature at higher voltages (0.7 V): the current initially rises at lower temperatures, but it decreases as the temperature increases above 200 K.

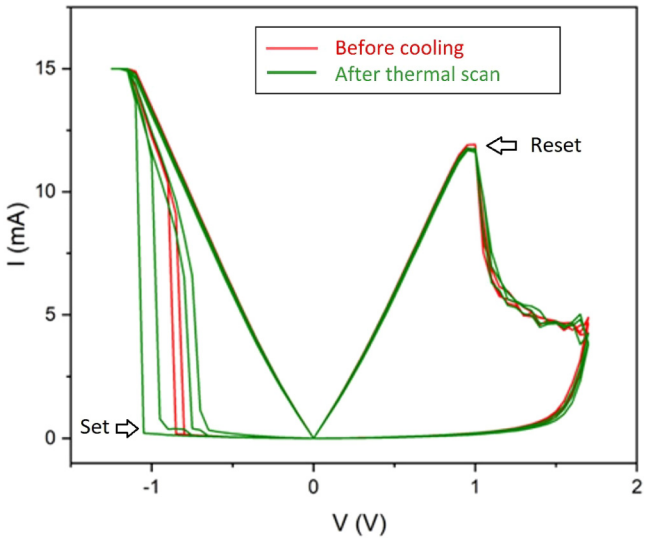

FIG. 1. Measured *I*–*V* curves at room temperature (300 K) before (red) and after (green) performing the experiment (*I*–*V* in the LRS is measured from 0 to 0.7 V, see Fig. 2). Clockwise resistive switching has been obtained, with the set (reset) at negative (positive) voltages.

IV. TEMPERATURE DEPENDENCE MODELING

The temperature dependence shown in Fig. 3(a) is consistent with the presence of a conductive filament (CF) of deep defect states,[11] with a semiconductor-like behavior that can be modeled

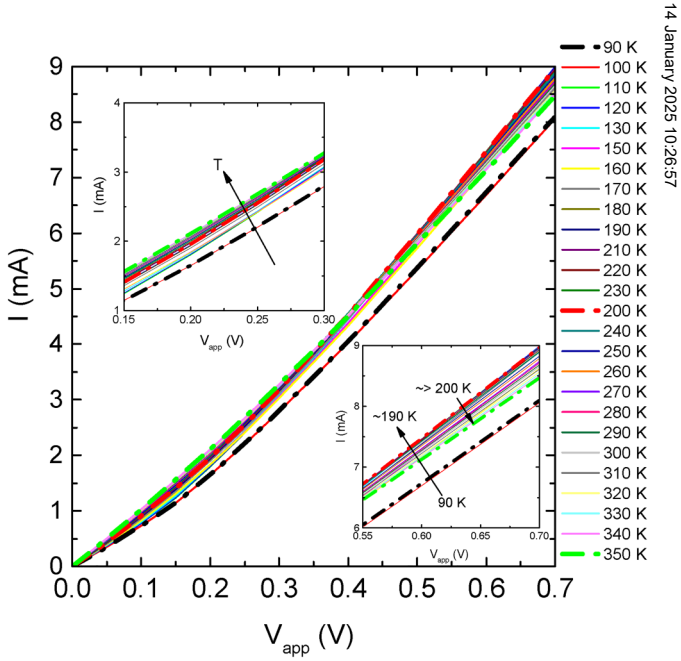

FIG. 2. Measured current vs applied voltage from 90 to 350 K. The insets show the zoomed views at low and high voltages. Different temperature dependences are observed at low voltages (inset on the left) and at high voltages (inset on the right). The *I*–*V* curves for three temperatures (90, 200, and 350 K) have been highlighted.

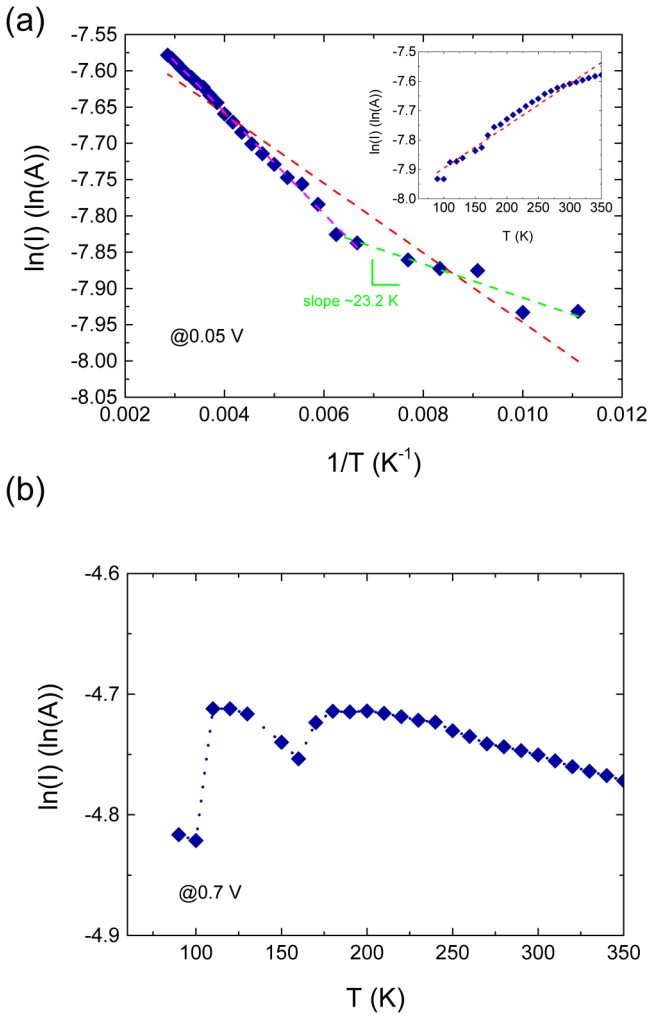

FIG. 3. (a) Measured current vs temperature (at an applied voltage of 0.05 V) in an Arrhenius format [ln(I) – (1/T)]. The data are not well fitted by a single linear trend (red dashed line), but different trends are observed. The inset shows the same current data vs the temperature. In this latter plot, a reduction of the curve slope can be observed at the highest temperatures. (b) Current vs temperature at an applied voltage of 0.7 V. A noticeable current increase is observed at low temperatures, as in the lower voltage case (a). However, a metallic-like behavior has been measured at higher temperatures, with a decreasing trend.

by a conductivity (σ) and the corresponding resistance (R) given by

$$\sigma(T) = \sigma_0 e^{-\frac{T_0}{T}} \Rightarrow R(T) = R_0 e^{\frac{T_0}{T}}. \quad (1)$$

Here, T is the device temperature, T_0 is an activation temperature for the conduction mechanism, and σ_0 and R_0 are the asymptotic conductivity and resistance at a temperature much higher than T_0. A value of $T_0 = 23.5$ K has been used for experimental data fitting (see Table I). This value is very close to that obtained from the slope of the current Arrhenius plot at the lowest temperatures

TABLE I. Model parameters.

Parameter	Value	Parameter	Value
I_0^*	0.6 mA	T_0	23.5 K
V_0	0.043 V	α	0.0016 K^{-1}
β	11.6×10^{-5} V/K	$T_r = T_b$	190 K
R_0	53.9 Ω	R_{Th}	2×10^3 K/W

[green dashed line in Fig. 3(a)]. The low activation energy (2.0 meV) indicates that the defects subband is very close to the Fermi level, as it was predicted by *ab initio* simulations[11] and rules out Poole–Frenkel conduction.[10] Therefore, although a temperature increase could ease the access to defect states, the corresponding temperature dependence is weak.[10,11,14] Low activation energies (close to zero) have also been previously reported for filaments with low resistance in NiO[12] and HfO_2[13] devices.

In addition to the ohmic conduction through the filament, the measured non-linear dependence has been modeled with the SM[16] in order to keep the model as simple as possible,

$$I = I_0 \times e^{-\frac{g}{g_0}} \times \sinh\left(\frac{V}{V_0}\right) = I_0^* \times \sinh\left(\frac{V_{app} - I \times R_{CF}(T)}{V_0}\right), \quad (2)$$

where I_0 is a current prefactor and g_0 and V_0 are fitting parameters.[16] V is the voltage drop across the gap and g is the gap width. In our experimental measurements, the filament does not change. Therefore, g remains constant, and for the sake of simplicity, we have grouped the first two factors in Eq. (2) in a single fitting parameter, I_0^*. The voltage in the gap, V, is calculated by extracting the voltage drop in the ohmic CF from the total applied voltage (V_{app}).[18] So, the CF resistance (R_{CF}) should also be calculated by taking its temperature dependence into account. The origin of this non-linear current dependence could be linked to a space (gap) between the CF tip and the Pt electrode, with a lower oxygen vacancies concentration whose length influences the device current because electrons have to tunnel through it.[10,11] According to *ab initio* simulations, not only the gap length but also the modulation of the potential barrier shape by empty (charged) oxygen vacancies determine the tunnel current through the gap.[11]

From Figs. 2 and 3(b), it turns apparent that from 190 to 200 K a new mechanism starts to gain relevance for higher temperatures, decreasing the total device conductance at larger voltages. This mechanism is supposed to be linked to the CF conduction and it has been modeled using a thermal positive coefficient (α) for the resistance,

$$R_{CF}(T) = \max(R(T), R(T) \times [1 + \alpha \times (T - T_r)]), \quad (3)$$

where R is the resistance given by Eq. (1), T_r is the temperature used to model this mechanism, and R_{CF} is the CF resistance at temperature T. The assumption that the origin of this current increase is related to the CF is coherent with the fact that this effect is more noticeable at higher voltages: the relative influence of the two conduction processes (ohmic and non-linear) changes with the applied voltage, and at higher voltages the resistance linked to the

non-linear component decreases. Therefore, the influence of the CF ohmic resistance is stronger and its temperature dependence is more apparent.

The activation of the CF conduction modeled by Eq. (1) is not enough for explaining the spreading of the curves at low voltages shown in Fig. 2. This fact is also supported by the graph shown in Fig. 3(a): the data are not aligned in the Arrhenius plot, but two different trends are observed. Therefore, another conduction effect (that makes the current grow as the temperature rises) is needed. This thermal dependence is more noticeable at the lowest voltages and, therefore, it is likely linked to the non-ohmic current component. In the context of the SM, this current increase can be modeled by means of a reduction of the V_0 parameter,

$$I = I_0^{*} \times \sinh\left(\frac{V}{V_0 - \beta\theta}\right), \tag{4}$$

where β is a fitting parameter and $\theta = \max(0, T - T_b)$, where T_b is also a fitting parameter and it corresponds to the temperature from which this equivalent barrier lowering starts to influence. This kind of linear dependence between a potential barrier and the temperature has been previously used in the context of the quantum point-contact model.[14,22,27,28] The origin of this thermal dependence could be related to the spreading of the electron energy distribution, which could make more traps accessible as the temperature rises. However, more research is necessary to clarify the underlying mechanism.

The measured thermal effects fit well the microscopic picture recently depicted by Funck and Menzel,[11] by means of *ab initio* simulations, for devices with deep defects.[11] In this case, defect states are induced by oxygen vacancies and spread over an energy range near the Fermi level, which could be linked to a conductive filament with a subband formation. Furthermore, the conduction is also influenced by tunneling across the energy barrier near the interface, being the tunneling barrier between the electrode and the available traps modulated by the screening of the potential by charged oxygen vacancies. In line with these results, we have observed a weak temperature dependence of the processes through the energy barrier because they do not require thermal excitation and a reduced temperature activated CF conduction takes place, which is compatible with defect states only slightly above the Fermi level. In addition, the high symmetry of the LRS in the 0–0.6 V range (Fig. 1) is also in line with the results expected for these devices.[11] Furthermore, the series resistance of the conductive filament contributes to more linear and symmetric I–V curves.

All the above temperature dependent conduction mechanisms have been implemented in a Spice subcircuit, which consists of a current source [Eq. (4)] in series with a resistor (R_{CF}), whose resistance depends on the temperature according to Eqs. (1) and (3). A simple circuital thermal model has been also considered[16,29] for calculating the device temperature with respect to the room temperature. We have observed that a high thermal resistance ($R_{th} > 10^4$ K/W) influences the simulated curves shape at high voltages; they bend down and separate from the experimental data that lie in a straight line at high voltages.

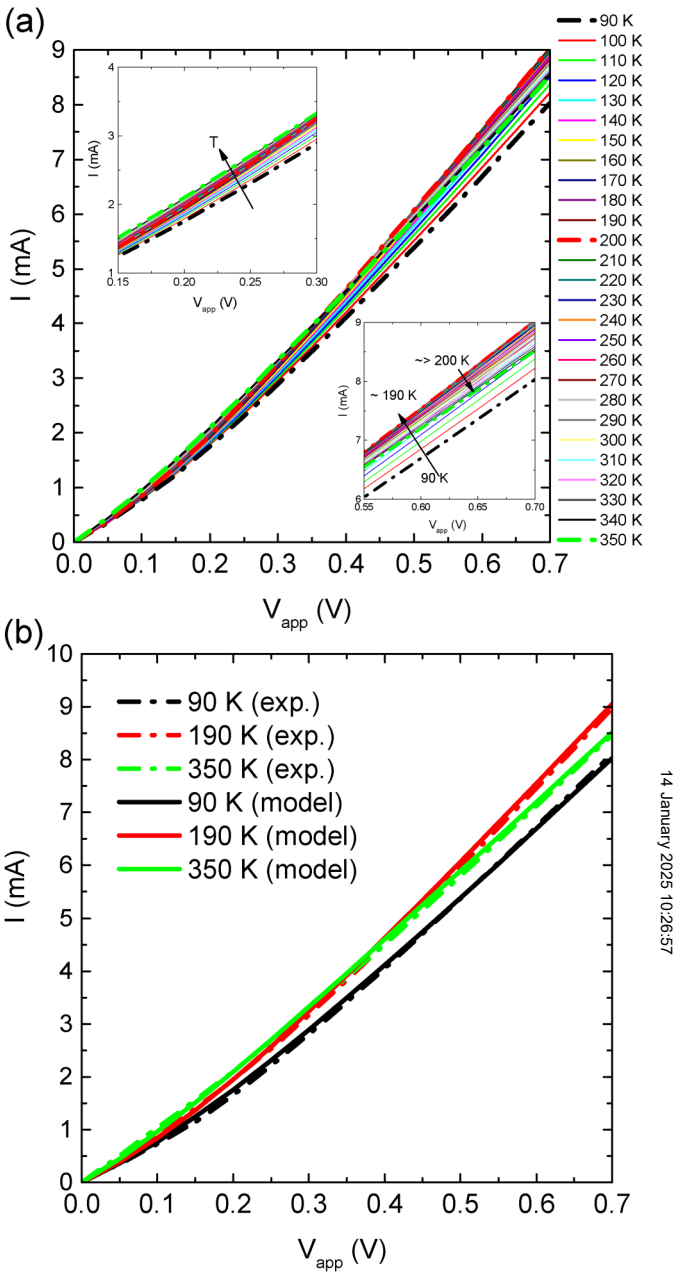

FIG. 4. (a) Modeled device current vs applied voltage for different temperatures from 90 to 350 K. The insets show zoomed views at low and high voltages, respectively. The temperature dependence observed at low voltages (inset on the left) and at the highest applied voltages (inset on the right) is correctly reproduced. (b) Modeled (solid lines) and experimental (dashed lines) I–V curves for 90, 190, and 350 K.

We have simulated I–V curves in LT-Spice [Fig. 4(a)] for all the experimentally considered external temperatures. The same trends observed in Fig. 2 are observed; for the sake of comparison, some representative curves are shown in Fig. 4(b). In order to

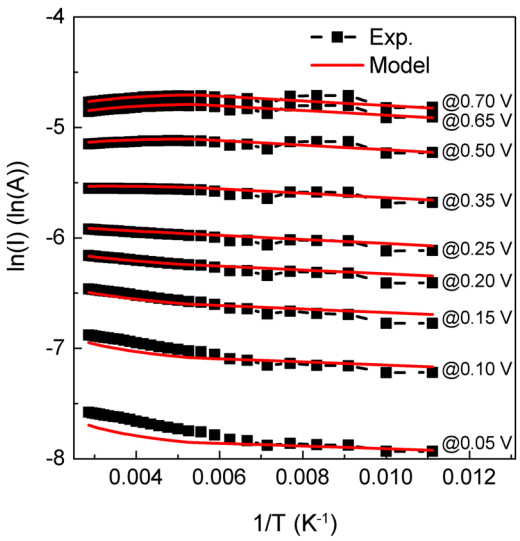

FIG. 5. Cuts across the *I–V* curves from Fig. 2 (measured current, squares and dashed lines) and Fig. 4(a) (simulated current, solid lines) at six different voltages are shown in an Arrhenius plot. A good agreement has been obtained, including the different temperature dependences shown at low and high voltages.

compare the experimental and modeled thermal dependences, Fig. 5 shows Arrhenius plots of the measured and simulated current at different applied voltages [that is, cuts from Figs. 2 and 4(a)]. In general, a good agreement between the simulated and measured data has been obtained. The model parameters are given in Table I.

Finally, as the studied devices exhibit non-linear *I–V* curves, the device resistance depends not only on the temperature, but also on the applied voltage. Figure 6 shows the experimental resistance (calculated as the applied voltage divided by the current) vs the temperature and applied voltage. In spite of the complex dependence represented by the colored surface that corresponds to the measured resistance, the simulated resistance (red balls) fits it remarkably well.

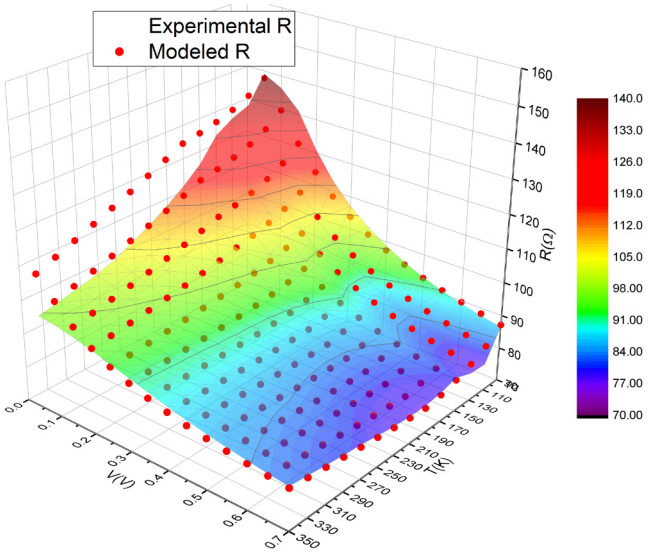

FIG. 6. Resistance (calculated as the applied voltage divided by the current) vs the applied voltage and the temperature. The colored surface corresponds to the experimental data, while the red balls are the modeled resistance calculated by simulation with LT-Spice.

V. CONCLUSIONS

Summing up, TiN/Ti/HfO_2/Pt resistive switching devices have been measured and modeled. Three different temperature dependent charge conduction effects have to be considered for modeling the experimental current in the LRS. Two of them are related to charge transport in a conductive filament linked to a high density of oxygen vacancies. A non-metallic enhancement of the conductivity with temperature described with a low activation energy was observed; on the other hand, once the conductivity increase is almost saturated, a metal-like conductance degradation is observed at the highest temperatures. Finally, a slight increase of the non-linear current component, as temperature rises, is also considered. This latter dependence is weak and this fact is a fingerprint of tunnel transitions instead of thermionic Schottky emission or Poole–Frenkel conduction mechanisms. The three conduction mechanisms have been implemented in a Spice-based compact model and the experimental results have been correctly fitted.

ACKNOWLEDGMENTS

This research was supported by the projects A-TIC-117-UGR18, B-TIC-624-UGR20, and IE2017-5414 funded by the Consejería de Conocimiento, Investigación y Universidad, Junta de Andalucía (Spain), and the FEDER program. The study was also supported by the European Regional Development Fund project "Emerging Orders in Quantum and Nanomaterials" (No. TK134) and the Estonian Research Agency (PRG753). M.B.G. acknowledges the Ramón y Cajal under Grant No. RYC2020-030150-I.

AUTHOR DECLARATIONS

Conflict of Interest

The authors have no conflicts to disclose.

Author Contributions

F. Jiménez-Molinos: Conceptualization (equal); Data curation (equal); Formal analysis (equal); Funding acquisition (equal); Investigation (equal); Methodology (equal); Writing – original draft (equal); Writing – review & editing (equal). **G. Vinuesa:** Conceptualization (equal); Data curation (equal); Investigation (equal); Writing – review & editing (equal). **H. García:** Conceptualization (equal); Data curation (equal); Investigation (equal); Writing – review & editing (equal). **A. Tarre:** Conceptualization (equal); Investigation (equal); Methodology (equal); Resources (equal); Writing – review & editing (equal).

A. Tamm: Conceptualization (equal); Investigation (equal); Methodology (equal); Resources (equal); Writing – review & editing (equal). **K. Kalam:** Conceptualization (equal); Investigation (equal); Methodology (equal); Resources (equal); Writing – review & editing (equal). **K. Kukli:** Conceptualization (equal); Investigation (equal); Methodology (equal); Resources (equal); Writing – review & editing (equal). **S. Dueñas:** Conceptualization (equal); Data curation (equal); Formal analysis (equal); Funding acquisition (equal); Investigation (equal); Methodology (equal); Writing – review & editing (equal). **H. Castán:** Conceptualization (equal); Data curation (equal); Formal analysis (equal); Funding acquisition (equal); Investigation (equal); Methodology (equal); Writing – review & editing (equal). **M. B. González:** Conceptualization (equal); Investigation (equal); Methodology (equal); Resources (equal); Writing – review & editing (equal). **F. Campabadal:** Conceptualization (equal); Funding acquisition (equal); Investigation (equal); Methodology (equal); Resources (equal); Writing – review & editing (equal). **J. B. Roldán:** Conceptualization (equal); Formal analysis (equal); Funding acquisition (equal); Investigation (equal); Methodology (equal); Writing – review & editing (equal).

DATA AVAILABILITY

The data that support the findings of this study are available from the corresponding author upon reasonable request.

REFERENCES

[1]M. Lanza, A. Sebastian, W. D. Lu, M. Gallo, M. F. Chang, D. Akinwande, F. M. Puglisi, H. N. Alshareef, M. Liu, and J. B. Roldan, "Memristive technologies for data storage, computation, encryption and radio-frequency communication," Science **376**(6597), 1–13, (2022).

[2]S. Yu, H. Jiang, S. Huang, X. Peng, and A. Lu, "Compute-in-memory chips for deep learning: Recent trends and prospects," IEEE Circuits Syst. Mag. **21**, 31–56 (2021).

[3]A. Chen, "Utilizing the variability of resistive random access memory to implement reconfigurable physical unclonable functions," IEEE Electron Device Lett. **36**, 138–140 (2015).

[4]S. Poblador, M. B. González, and F. Campabadal, "Investigation of the multilevel capability of TiN/Ti/HfO_2/W resistive switching devices by sweep and pulse programming," Microelectron. Eng. **187-188**, 148–153 (2018).

[5]H. García, S. Dueñas, O. G. Osorio, and H. Castán, "Current pulses to control the conductance in RRAM devices," IEEE J. Electron Devices Soc. **8**, 291–296 (2020).

[6]M. Witzleben, S. Wiefels, A. Kindsmüller, P. Stasner, F. Berg, F. Cüppers, S. Hoffmann-Eifert, R. Waser, S. Menzel, and U. Böttger, "Intrinsic RESET speed limit of valence change memories," ACS Appl. Electron. Mater. **3**, 5563–5572 (2021).

[7]C. Mahata, C. Lee, Y. An, M.-H. Kim, S. Bang, C. S. Kim, J.-H. Ryu, S. Kim, H. Kim, and B.-G. Park, "Resistive switching and synaptic behaviors of an HfO_2/Al_2O_3 stack on ITO for neuromorphic systems," J. Alloys Compd. **826**, 154434 (2020).

[8]D. Ielmini and R. Waser, *Resistive Switching: From Fundamentals of Nanoionic Redox Processes to Memristive Device Applications* (Wiley-VCH, 2015).

[9]C. Mahata and S. Kim, "Modified resistive switching performance by increasing Al concentration in HfO_2 on transparent indium tin oxide electrode," Ceram. Int. **47**, 1199–1207 (2021).

[10]S. Yu, X. Guan, and H.-S. P. Wong, "Conduction mechanism of TiN/HfO_x/Pt resistive switching memory: A trap-assisted tunneling model," Appl. Phys. Lett. **99**, 063507 (2011).

[11]C. Funck and S. Menzel, "Comprehensive model of electron conduction in oxide-based memristive devices," ACS Appl. Electron. Mater. **3**, 3674–3692 (2021).

[12]D. Ielmini, F. Nardi, and C. Cagli, "Physical models of size-dependent nanofilament formation and rupture in NiO resistive switching memories," Nanotechnology **22**, 254022 (2011).

[13]S. Long, X. Lian, C. Cagli *et al.*, "Quantum-size effects in hafnium-oxide resistive switching," Appl. Phys. Lett. **102**, 183505 (2013).

[14]L. M. Prócel, L. Trojman, J. Moreno, F. Crupi, V. Maccaronio, R. Degraeve, L. Goux, and E. Simoen, "Experimental evidence of the quantum point contact theory in the conduction mechanism of bipolar HfO_2-based resistive random access memories," J. Appl. Phys. **114**, 074509 (2013).

[15]E. Miranda and J. Suñé, "Analytic modeling of leakage current through multiple breakdown paths in SiO_2 films," in *2001 IEEE International Reliability Physics Symposium Proceedings* (IEEE, 2001), pp. 367-379.

[16]X. Guan, S. Yu, and H.-S. P. Wong, "A SPICE compact model of metal oxide resistive switching memory with variations," IEEE Electron Device Lett. **33**, 1405–1407 (2012).

[17]P. Huang *et al.*, "A physics-based compact model of metal-oxide-based RRAM DC and AC operations," IEEE Trans. Electron Devices **60**, 4090–4097 (2013).

[18]D. Maldonado, F. Aguirre, G. González-Cordero, A. M. Roldán, M. B. González, F. Jiménez-Molinos, F. Campabadal, E. Miranda, and J. B. Roldán, "Experimental study of the series resistance effect and its impact on the compact modeling of the conduction characteristics of HfO_2-based resistive switching memories," J. Appl. Phys. **130**, 054503 (2021).

[19]Y. Matveyev, K. Egorov, A. Markeev, and A. Zenkevich, "Resistive switching and synaptic properties of fully atomic layer deposition grown TiN/HfO_2/TiN devices," J. Appl. Phys. **117**, 044901 (2015).

[20]C. Ahn, S. Kim, T. Gokmen, O. Dial, M. Ritter, and H.-S. P. Wong, "Temperature-dependent studies of the electrical properties and the conduction mechanism of HfO_x-based RRAM," in *Proceedings of Technical Program—2014 International Symposium on VLSI Technology, Systems and Application (VLSI-TSA)* (IEEE, 2014), pp. 1–2.

[21]R. Fang, W. Chen, L. Gao, W. Yu, and S. Yu, "Low-Temperature characteristics of HfO_x-based resistive random access memory," IEEE Electron Device Lett. **36**, 567–569 (2015).

[22]C. Walczyk, D. Walczyk, T. Schroeder, T. Bertaud, M. Sowinska, M. Lukosius, M. Fraschke, D. Wolansky, B. Tillack, E. Miranda, and C. Wenger, "Impact of temperature on the resistive switching behavior of embedded HfO_2-based RRAM devices," IEEE Trans. Electron Devices **58**, 3124–3131 (2011).

[23]K.-M. Kim, J. S. Jang, S.-G. Yoon, J.-Y. Yun, and N.-K. Chung, "Structural, optical and electrical properties of HfO_2 thin films deposited at low-temperature using plasma-enhanced atomic layer deposition," Materials **13**, 2008 (2020).

[24]K. Kukli, M. Ritala, T. Sajavaara, J. Keinonen, and M. Leskelä, "Atomic layer deposition of hafnium dioxide thin films from hafnium tetrakis(ethylmethylamide) and water," Chem. Vap. Deposition **8**, 199–204 (2002).

[25]K. Xiong, J. Robertson, M. C. Gibson, and S. J. Clark, "Defect energy levels in HfO_2 high-dielectric-constant gate oxide," Appl. Phys. Lett. **87**, 183505 (2005).

[26]G. Vinuesa, H. García, M. B. González, K. Kalam, M. Zabala, A. Tarre, K. Kukli, A. Tamm, F. Campabadal, J. Jiménez, H. Castán, and S. Dueñas, "Effect of dielectric thickness on resistive switching polarity in TiN/Ti/HfO_2/Pt stacks," Electronics **11**, 479 (2022).

[27]A. Avellán, E. Miranda, and D. Schroeder, "Model for the voltage and temperature dependence of the soft breakdown current in ultrathin gate oxides," J. Appl. Phys. **97**, 014104 (2005).

[28]M. Calixto, D. Maldonado, E. Miranda, and J. B. Roldán, "Modeling of the temperature effects in filamentary-type resistive switching memories using quantum point-contact theory," J. Phys. D: Appl. Phys. **53**, 295106 (2020).

[29]J. B. Roldán, G. González-Cordero, R. Picos, E. Miranda, F. Palumbo, F. Jiménez-Molinos, E. Moreno, D. Maldonado, S. B. Baldomá, M. M. Al Chawa, C. de Benito, S. G. Stavrinides, J. Suñé, and L. O. Chua, "On the thermal models for resistive random access memory circuit simulation," Nanomaterials **11**, 1261 (2021).